Proceedings World Geothermal Congress 2020+1
Reykjavik, Iceland, April - October 2021

Multi-scale Unsupervised Machine Listening to Geothermal Earthquakes in the Geysers, CA

Ben Holtzman[1]*, Felix Waldhauser[1], John Paisley[2], Patricia Martinez-Garzon[3], Grzegorz Kwiatek[3], Arthur Paté[4], Lapo Boschi[5], Nicolas Van der Elst[6], Sierra Boyd[7], Doug Dreger[7]

[1]*Lamont Doherty Earth Observatory, Columbia Univ. 61 Rt. 9W, Palisades, NY 10964. [2]Data Science Institute, Columbia University, [3]GFZ Potsdam, Germany, [4]ISEN, Lille, France, [5]Uni. Padua, Italy, [6]USGS, Pasadena, [7]Berkeley Seismological Laboratory, UC Berkeley.

*benh@ldeo.columbia.edu

Keywords: Induced Seismicity, Machine Learning, Geothermal Reservoir Mechanics, Data Analytics.

ABSTRACT

Understanding seismicity patterns in geothermal reservoirs can be an important source of information on the thermodynamic state and geomechanical changes in the reservoir. Here, we apply unsupervised machine learning (feature extraction and clustering) to earthquakes in The Geysers geothermal reservoir in Northern California. The feature extraction approach is comprised of sequential non-negative matrix factorization (NMF) and hidden Markov modeling (HMM), which together reveal subtle spectral differences in among earthquakes. Fingerprints generated from the HMM results are then clustered using k-means. We search empirically for correlations of the clusters with physical aspects of the earthquakes, such as spatial locations, moment tensor components, or event times. In our first study, we found that strong clustering emerged from analysis of 46,000 earthquakes over the entire Geysers region in three years. These clusters formed no clear spatial patterns but very strong temporal patterns, essentially defining seasonal earthquakes types that recur annually, closely correlating with average fluid injection rates. In order to better understand these patterns, we analyze three more data sets: (1) Zooming out in time, 12 years of seismicity over the entire Geysers area; (2) Zooming in in space, to a small area in the NW Geysers, over a 7-year period, and (3) an adjacent smaller area in the NW where experiments in enhanced geothermal systems (EGS) were performed. These analyses are currently works-in-progress, but initial results from (2) reveal no apparent correlations with moment tensor properties (all types of moment tensors occur in each cluster). In all 3, we find strong temporal correlations, but with higher resolution in the correlations between injection rate and clustering. This result strengthens our inference that changes in the thermal-mechanical state (stress changes associated with water and steam content and distribution on fault interfaces) causes subtle variations in seismic source spectra. Sonic representations (sonification) of the seismic data aid in the interpretation of the machine listening results.

1. INTRODUCTION

Understanding seismicity patterns in geothermal reservoirs can be an important source of information on changes in the thermomechanical conditions in the reservoir. Any such information can be useful for mitigating seismicity, understanding fluid and vapor pathways and improving reservoir productivity. In 2018, we published a study applying unsupervised machine learning (in our case, feature extraction and statistical clustering) analysis of three years of earthquakes in The Geysers geothermal reservoir in Northern California (Holtzman et al., 2018, referred to as H18 within). In that study, we found that strong clustering emerged from analysis of 46,000 earthquakes over the entire Geysers region in three years. These clusters formed no clear spatial patterns but very strong temporal patterns, essentially defining seasonal earthquake types that recur annually, closely correlating with average fluid injection rates over the entire reservoir. Winter earthquakes correlate strongly with peak average injection rates of fluid into the reservoir, while Summer and Fall earthquakes correlate with minima in injection rates. While the correlation to fluid injection rate is strong, we do not know why that correlation exists. Is it because the injected fluid (a) changes the stress state on faults, (b) changes in the frictional properties and/or asperity distribution, or (c) fluid and vapor ratios in fractures changes the scattering and attenuative properties of the propagation path between source and station? It may well be that injection causes all of these changes to happen simultaneously, so our goal may not be to distinguish among them, but to be able to characterize the ensemble changes in the reservoir state from the subtle differences in the seismic spectra.

In order to better understand the physical causes of the spectral changes that are reflected in the clustering results, a first approach is to focus in on local regions where seismicity can be related to injection and production histories from a small number of injection wells. We can build on the numerous detailed studies of the seismicity in the Geysers using established methods for identifying moment tensors and other physical aspects of the seismicity, to add possible sources of correlation with clustering. This paper represents our first effort to seek correlations between detailed moment tensor studies and our ML clustering results.

2. METHODS

In the following, we first describe the ML methods, and then the data sets that we will analyze.

2.1 Machine Learning methods

Seismology can and is benefiting rapidly from the explosion of new machine learning (ML) methods. Most current efforts in application of ML in seismology are in detection and classification, e.g. Bergen et al. (2019). We use a very different approach that is possible only after an earthquake catalog has been built, referred to as unsupervised feature extraction (UFE), developed in H18, and illustrated in Fig 1. The aim is to discriminate among events by characterizing subtle differences between the spectra of each

event, and then finding events that have similar patterns in their spectral differences. To clarify, the first part of the method (Fig. 1b), non-negative matrix factorization (NMF) “learns” a dictionary of features that are common to all signals and a corresponding

"activation matrix" that is unique to each signal. The product of the dictionary and activation matrix is a close approximation to the original spectrogram. Because we are interested in the differences among signals, only the activation matrixes are used in subsequent steps. The HMM (Fig 1c) seeks hidden features or "states" in the time series data of the activation matrix, where states characterized by frequency features that are co-occurring. Thus, the HMM reveals patterns hidden in the data that we would likely not identify otherwise. The output of the HMM is a emissions matrix that shows how each state is characterized by different ensembles of frequency features, like the NMF dictionary, and the state sequence matrix that is the time-activation of states. Interestingly, in the example in Fig. 1c , the coda after the event is characterized by only 2-3 states for a short duration and then settles in to a more complex pattern. In comparison, in the NMF activation matrix, the earthquake itself is barely visible. The HMM's finding of hidden states allows the impulsive event to re-emerge. The state sequence matrix is then converted to a fingerprint by counting the transitions between states. The NMF features and the HMM states are also achieving significant dimensionality reduction, reducing a 600x300 spectrogram to a 15x15 fingerprint. We call the ensemble algorithm "SpecUFEx" (Unsupervised Spectral Feature Extraction), and the codes are available on github (https://github.com/benholtzman).

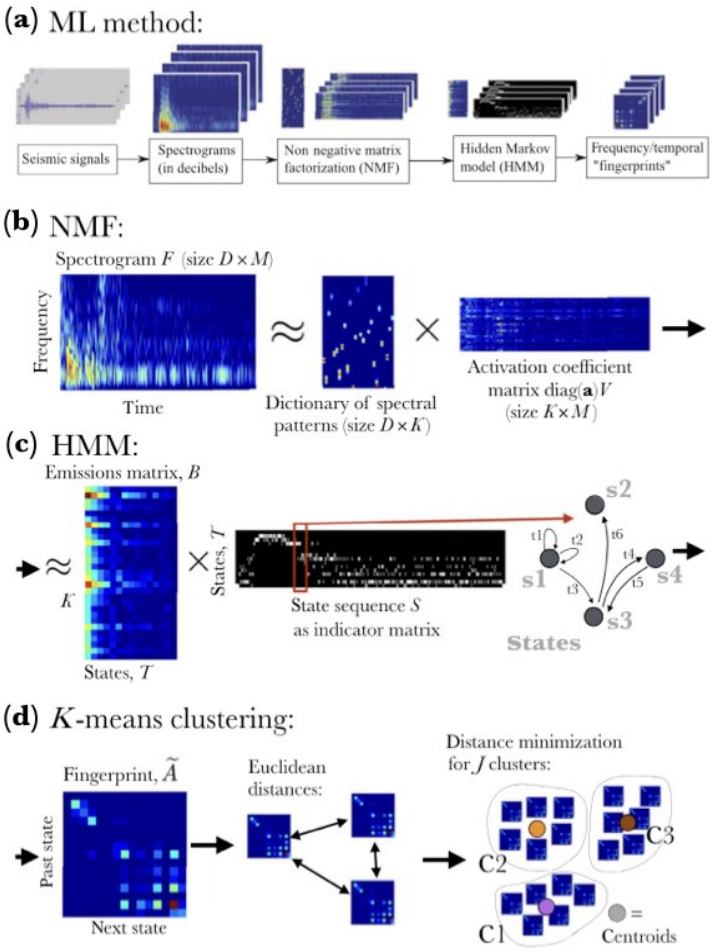

Figure 1. Machine Learning methods (unsupervised spectral feature extraction), described in the text.

The fingerprints can then be analyzed in a wide range of ways. In our first and this paper, we use the old and venerable clustering algorithm "k-means", in which trial centroids are randomly seeded and Euclidean distances from each centroid to each event are calculated, and then moved and updated until the sum of Euclidean distances is stable and minimal. One only specifies the number of clusters. Here, we use J = 2-20, and then look for the smallest number that captures the apparent variability. More quantitative methods for visually and algorithmically choosing the most meaningful number of centroids is underway.

Both the feature extraction and the clustering are fully unsupervised steps, so the next steps are empirical and/or hypothesis driven comparison of cluster data to other parameters. In this paper, we compare to a range of aspects of the moment tensors calculated by, for example, Martínez-Garzón et al., 2013, 2014) and Kwiatek et al., (2015).

2.2 Data sources

Earthquake catalogs and data are assembled from the Northern California Earthquake Data Center (https://ncedc.org/), for M> 0.1, for the following time and map windows:

(1) Whole Geysers Region: 9 years of all earthquakes M> 0.1 in the Geysers region (2006-2015), shown in Fig 2, for stations STY and SQK.

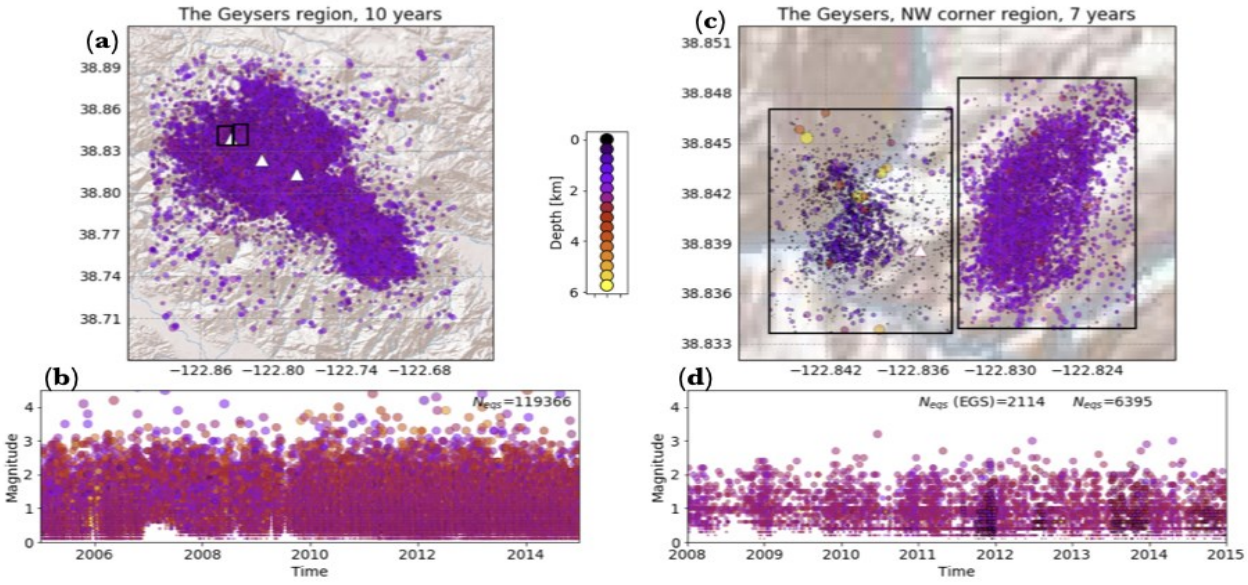

Figure 2: (a) The whole Geysers geothermal region and (b) 10 years of seismicity. Black squares show the two NW sub-regions. White triangles show the seismic stations (AL4, SQK, STY from left to right). (c) Seismicity (magnitude vs time) for the two sub-regions in the NW area around AL4. The smaller catalog (left) is the EGS study area. (d) Seismicity for the two catalogs (black rimmed events are in the smaller EGS catalog.

(2) Northwest Geysers region 1: 7 years (2008-2014) of events in the local region surrounding injection wells Prati 9 and 29, shown in the black square in Fig 5, for station AL4.

(3) Northwest Geysers region 2 (EGS area): 7 years (2008-2014) of events in the local region around the Prati 32 injection well (the EGS study area), for station AL4, as studied in detail by, for example, Boyd et al., 2018. In this local region, the injection rate varies less seasonally than the other areas, according to the design of the EGS demonstration experiment, described in Garcia et al., 2016.

For all catalog events (for which data is available), we download 500 Hz waveform data for 20 seconds, starting 1 second before the event arrival time at the station. We apply the instrument response, detrend and demean the data, and then calculate the spectrogram for each event. Waveforms and spectrograms for randomly selected events are visually inspected for obvious problems. Spectrograms are trimmed above ~200 Hz. The spectrograms are then analyzed with the SpecUFEx method.

3. RESULTS

3.1 The whole Geysers reservoir, 10 years.

This data set is the same area as that in Holtzman et al. (2018), but over a 10-year time window (9 shown). The 3 years analyzed in our first study (H2018) are shown in the purple box in Fig. 3. As in that study, we found no obvious spatial patterns, but very strong temporal patterns: a 9-year repetition of the pattern in the whole Geysers area. That is, each cluster is associated with large concentrations of events in different repeating temporal windows. The windows for each cluster correlate strongly with different phases in the fluid injection history, primarily maxima and minima, that correspond to seasonal changes in volumes of street runoff water from nearby cities. The results here are shown for 4 clusters only.

3.2 NW Geysers locality

The new data analyzed here come from the vicinity of Prati 9 and 29 injection holes, and have been studied in great detail by, for example, Martínez-Garzón et al, (2013, 2014) and Kwiatek et al. (2015). First, the injection history from the two wells provides a useful semi-controlled experiment, in which Prati 9 was operative throughout the study period, but Prati 29 turned on only in early 2010 and off in late 2013, as shown in Fig 4. The change had significant effect on the seismicity patterns, and on the spectral changes picked up by our ML methods. For the rest of this paper, we show the results for 6 clusters. The spatial patterns in the clustering are not strong, in that there is overlap for all clusters, shown in map (Fig 5a) and cross section view (Fig. 5b). In both, the bottom of drill holes Prati 9 and 29 are shown in red and yellow squares respectively. Interestingly, when Prati 29 turns on, the bulk of the seismicity is still around the Prati 9 borehole bottom. Fig. 5c shows the distance of each event from the P9 borehole bottom as a function of time, colored by cluster. While there is a large spread during high injection periods, again, there does not appear to be a strong spatial association of any cluster, in this case with distance from the borehole bottom. However, the temporal patterns are very clear. The cluster (#2) in light purple shows a clear association with the turning on of Prati 29. The other clusters somewhat less clear temporal patterns, but still hold to the basic association of a certain cluster with a phase of the injection rate, as shown in Figure 6. Clusters 1,3,5 are associated with the peaks in injection rate before Prati 29 turns on, but then diminish in the aftermath. Cluster 2 is on for only one year, almost exclusively, and then turns off and is replaced by activity in 4 and 6, but 1,3,5 return as well. This recurrence

after a hiatus suggests that after an initial (thermal and/or hydraulic) shock to the reservoir, it returned to a previous state, if that is what is characterized by subtle differences in the seismic spectra.

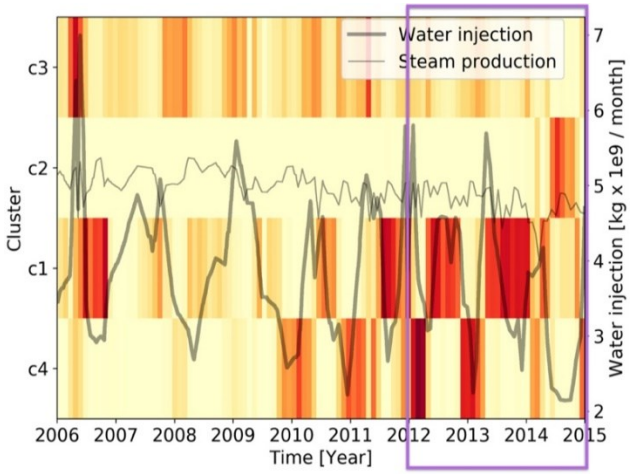

Figure 1: "Spistogram" (temporal histograms for each cluster) for 9 years of data over the whole Geysers area (data from station SQK). The histograms for each cluster are normalized to give equal area density (integral of each histogram=1) so there is no absolute color scale; pale yellow (~0) to deep red (max) represents increasing number of events in that bin.

In the following, we test for correlations among clusters and moment tensor properties, from the studies of Martínez-Garzón et al, (2013, 2014) and Kwiatek et al. (2015) for 726 events. In Figure 7b, it is clear that Cluster 3 contains most of the larger events, M>1.5, except for 2010, when Cluster 2 took almost all events. In 7c and 7d, the vertical streaks of dots of similar color indicate that the clusters are not strongly correlated with the volumetric or DC components of the moment tensors. Finally, in Figure 8, we show results of fault type (normal, strike slip, or thrust/reverse) as a function of cluster. Again, there does not seem to be strong correlation between fault type and cluster. The large variations are in total number, but the relative proportions do not change very much, and the uncertainties in each orientation determination are not shown.

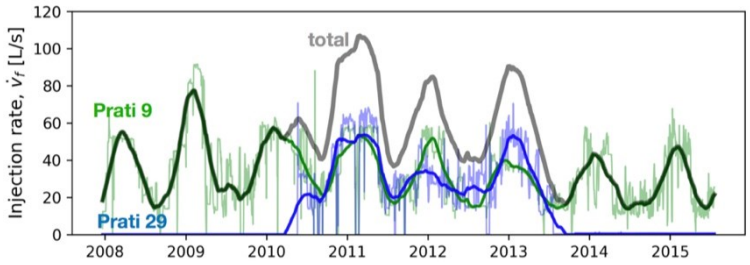

Figure 2: Injection history in Prati 9,29 area

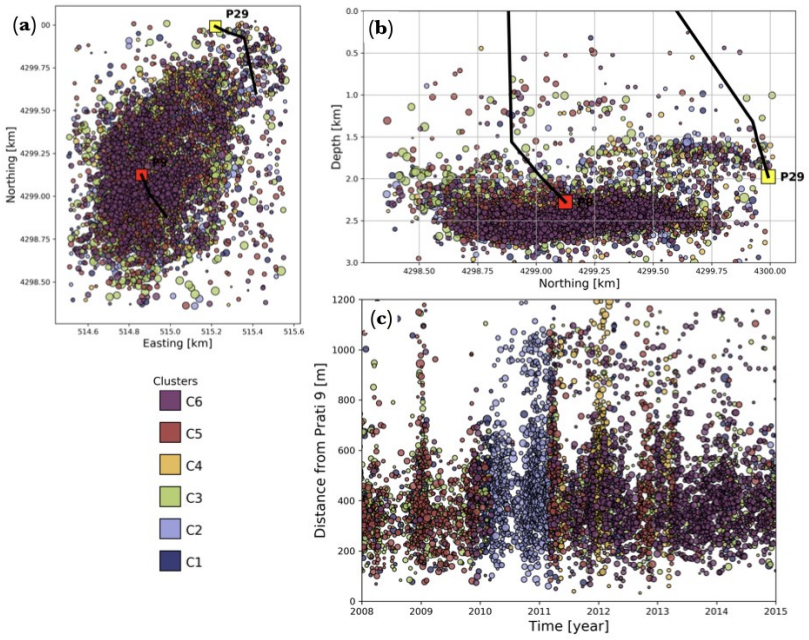

Figure 3: (a) Map view of seismicity in 6 clusters. (b) Cross section view of seismicity in 6 clusters. (c) time series of distance of each event from the bottom of Prati 9 borehole (red square).

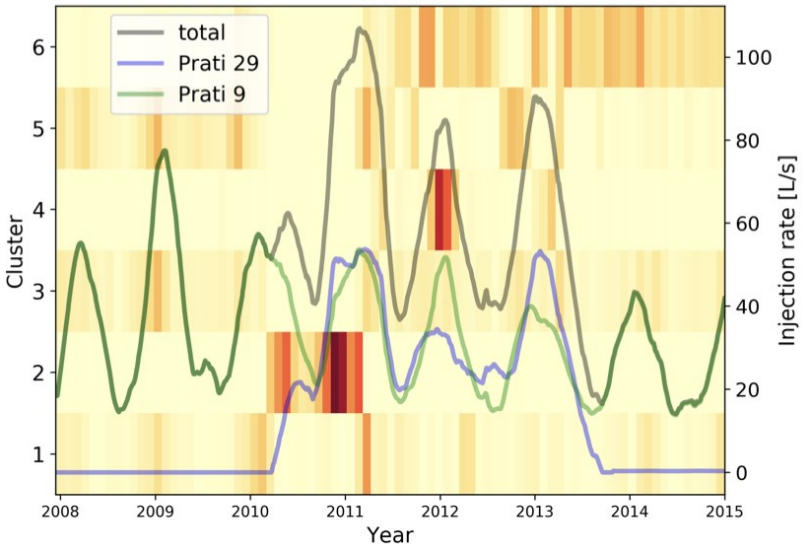

Figure 6: Spistogram of cluster activity (number of earthquakes in each time window in each cluster), for 6 clusters in the vicinity of Prati 9 and 29 over 7 years.

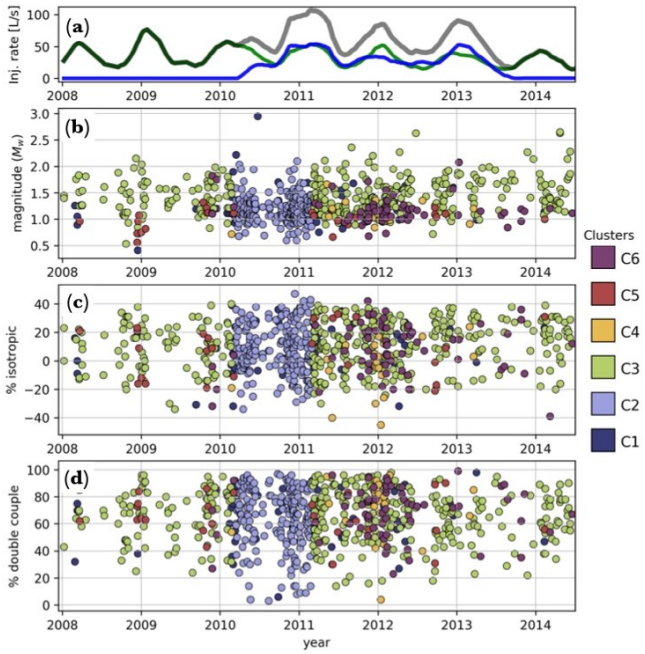

Figure 7: Temporal variations in moment tensor properties vs time and cluster number. (a) injection history in Prati 9 and 29, (b) Magnitude, (c) % isotropic, (d) % double couple.

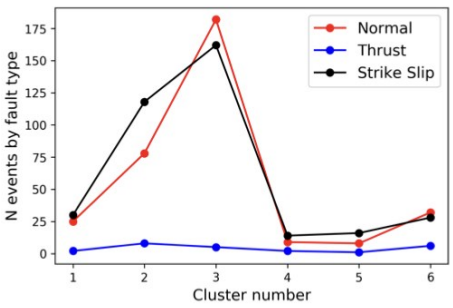

Figure 4: Fault orientation as a function of cluster.

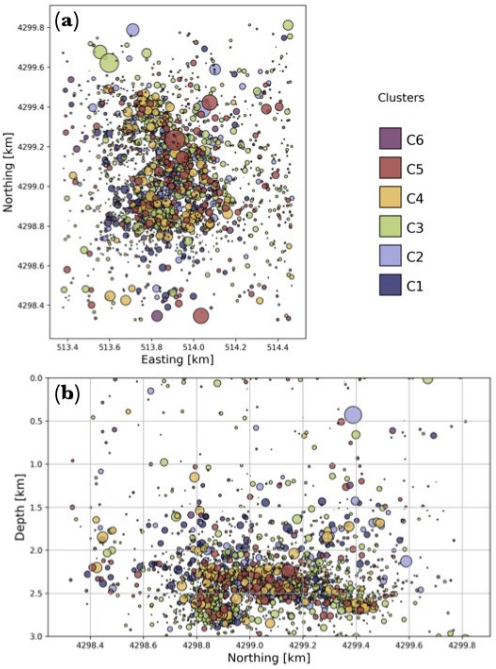

Figure 9: (a) Map view of seismicity in 6 clusters. (b) Cross section view of seismicity in 6 clusters.

3.3 NW EGS study area.

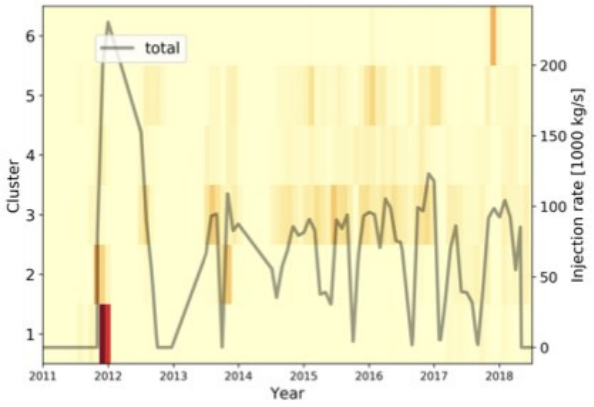

Figure 10: Spistogram of UFE clusters (6) from the NW EGS site, same data as in Fig. 9.

The SpecUFEx methods have been applied to this smaller catalog, with results shown for 6 clusters. Map and cross section views of the events colored by cluster is shown in Fig. 9a. Again, no clear spatial patterns appear at the map scale, nor with depth, where most events for all clusters occur between 1.5-3 km. We did not have access to the exact borehole locations to perform the same analyses as for the Prati-9/29 area. The spistogram in Fig. 10, shows a very strong association of Cluster 1 with the onset of fluid injection (and a lesser extent C2) in 2012. Apart from the onset of injection in 2012, C3 is strongly associated with the higher injection periods, while C5 is associated with relative drops in injection rate in those periods (over 2013-2018). By design, these periods are much less coupled to seasonal variations in the water supply than anywhere else in the Geysers region.

(Note that there is no necessary relation between C1 of this area and C1 of the P9/29 area; cluster numbers are arbitrary and apply only within each learning analysis. If we performed the learning on these two NW areas combined, we would be able to associate clusters. We leave this exercise for near future work.)

4. CONCLUSIONS AND FURTHER QUESTIONS

The general aim of our study is to better understand what the unsupervised feature extraction method is able to reveal about the nature of variations in seismicity. Being unsupervised, we do not know the associations *a priori*, so we search for possibilities. As shown above, from the analysis of the P9-29 NW area, there is no clear association between moment tensor properties and cluster, suggesting that the spectral differences associated with each cluster do not strongly reflect variations in the macroscopic or location orientations of the stress state, nor simply the radiation patterns associated with the orientation of the event relative to the station. Because most of the variations in the moment tensor properties are occurring simultaneously (all types occur all the time), but the clusters are associated with different temporal windows, the lack of correlation is not surprising. We cannot support the hypothesis that clustering reflects changes in the moment tensor, but more rigorous statistical tests will be undertaken.

Another possibility is that the clustering simply reflects variations in the acoustic properties of the reservoir without any direct information on the rupture processes of the earthquakes. In H18, we argued against effects of fluid/steam ratios in the porosity/fractures on the bulk or shear attenuation in the reservoir, at least to the magnitude that would cause significant attenuation of the higher frequencies in the measured spectra, because if that effect were dominant, we would see spatial patterns in the clustering with distance from the seismic station. We do not see that kind of pattern at all. However, the effects of attenuation could be more subtle. To push this further, in one experiment not shown here, we analyzed time windows of waveforms that occurred one hour before each event in the catalog (3 years, whole Geysers area), to test this possibility that the variations are more associated with reservoir properties than with the raw earthquake source spectra. It is far from an ideal experiment because the noise is generated at least in part by microseismicity that is undetectable as discrete events by standard methods, but those events would likely have the same variations in their rupture process or frictional properties that larger events would have. That said, we see roughly the same general temporal clustering patterns but with significantly more diffuse peaks in their temporal histograms. This result is consistent with the idea that the variations in spectra are coming from the earthquake sources, not from the path.

These results reinforce the idea that the spectral differences are associated with fine scale variations in the nature of the fault surfaces with changes in temperature and fluid/vapor ratios, reflecting microscopic variations in friction and possibly asperity distribution. Changes in these surface properties would also likely affect wave propagation (attenuation) as well, but not as the primary cause of spectral variations.

We are developing methods to visualize the actual differences in the spectral (spectrograms) that lead to separation into different clusters. These will be applied to these datasets (before the conference presentation), but were not finished at the time of submission. These visual (and sonic) comparisons will help us articulate hypotheses on the variations in physical processes causing spectral variations. Further studies will also treat 3-channel data, to gain further insight into the correlations (or lack thereof) with moment tensor orientation, and perhaps simply improve the richness of characterization and clustering by tripling the amount of (correlated) information going into the UFE analysis.

5. ACKNOWLEDGEMENTS

Water injection and steam production data come from the following CA Dept. of Conservation sites: https://secure.conservation.ca.gov/GeoSteam/GeoWellSearch/WellDetails?apinum=09790599, 09790630, for for Prati 32 and 31 respectively. Seismic data comes from IRIS and NCEDC.

REFERENCES

Bergen, K. J., Johnson, P. A., Maarten, V., & Beroza, G. C. (2019). Machine learning for data-driven discovery in solid Earth geoscience. *Science*, 363(6433), eaau0323.

Boyd, O. S., Dreger, D. S., Gritto, R., & Garcia, J. (2018). Analysis of seismic moment tensors and in situ stress during Enhanced Geothermal System development at The Geysers geothermal field, California. *Geophysical Journal International*, 215(2), 1483-1500.

Garcia, J., Hartline, C., Walters, M., Wright, M., Rutqvist, J., Dobson, P. F., & Jeanne, P. (2016). The Northwest Geysers EGS demonstration project, California: Part 1: characterization and reservoir response to injection. *Geothermics*, *63*, 97-119.

Holtzman, B. K., Paté, A., Paisley, J., Waldhauser, F., & Repetto, D. (2018). Machine learning reveals cyclic changes in seismic source spectra in Geysers geothermal field. *Science advances,* 4(5), eaao2929.

Jeanne, P., Rutqvist, J., Dobson, P. F., Garcia, J., Walters, M., Hartline, C., & Borgia, A. (2015). Geomechanical simulation of the stress tensor rotation caused by injection of cold water in a deep geothermal reservoir. *Journal of Geophysical Research: Solid Earth*, *120*(12), 8422-8438.

Kwiatek, G., Martínez-Garzón, P., Dresen, G., Bohnhoff, M., Sone, H., & Hartline, C. (2015). Effects of long-term fluid injection on induced seismicity parameters and maximum magnitude in northwestern part of The Geysers geothermal field. *Journal of Geophysical Research: Solid Earth,* 120(10), 7085-7101.

Martínez-Garzón, P., Bohnhoff, M., Kwiatek, G., & Dresen, G. (2013). Stress tensor changes related to fluid injection at The Geysers geothermal field, California. *Geophysical Research Letters,* 40(11), 2596-2601.

Martínez-Garzón, P., Kwiatek, G., Sone, H., Bohnhoff, M., Dresen, G., & Hartline, C. (2014). Spatiotemporal changes, faulting regimes, and source parameters of induced seismicity: A case study from The Geysers geothermal field. *Journal of Geophysical Research: Solid Earth,* 119(11), 8378-8396.